RGNZ/MGPB

Geomechanical Impacts of Pore Types Identified by Machine Learning in Permian–Triassic Reservoirs of the Persian Gulf

Rudarsko-geološko-naftni zbornik
(The Mining-Geology-Petroleum Engineering Bulletin)
DOI: 10.17794/rgn.2026.5.4

Original scientific paper

Saeed Karimkhani[1] ✉, **Vahid Tavakoli**[1]* ✉
School of Geology, College of Science, University of Tehran, Tehran, Iran.

Abstract
Understanding geomechanical behaviour is essential in the petroleum industry for optimizing wellbore stability, drilling operations, and hydrocarbon recovery. This study examines how different pore types influence the geomechanical properties of the reservoir. Petrographic analysis, wireline logs, routine core data, and geomechanical measurements were used. Geomechanical data include Young's modulus (E), Poisson's ratio (ϑ), shear modulus (G), bulk modulus (K), Schmidt hammer rebound values, unconfined compressive strength (UCS), cohesion (C), and internal friction angle (Φ). The DataFrame was divided based on porosity to evaluate its impact on geomechanical properties. Missing porosity values were predicted using the ExtraTreesRegressor model, which achieved an R^2 of 0.82. Since the datasets had different sampling depths, the radial basis function (RBF) method was used to interpolate wireline-log geomechanical properties to core depths. Machine-learning-based barplots were then applied to assess how pore types affect geomechanics. The results show that rocks with non-fabric-selective pores have the highest geomechanical strength. In contrast, samples with fabric-selective pores exhibit the weakest properties. Depositional pore types fall in between, having lower geomechanical properties than non-fabric-selective pores, but higher than fabric-selective ones. By integrating petrographic and petrophysical data with machine-learning techniques, this study provides a practical workflow for evaluating geomechanical heterogeneity. This approach improves reservoir characterization and supports better development decisions in carbonate fields.

Keywords:
pore type; geomechanical; properties; machine learning; ExtraTreesRegressor model

1. Introduction

Geomechanics plays a key role in managing stress-sensitive formations and addressing subsurface challenges in the petroleum industry (**Hamid et al., 2017; Akbarzadeh et al., 2026**). It affects many operations, including drilling, completion, production, and reservoir engineering (**Settari and Sen, 2008**). Geomechanical understanding is also essential for hydraulic fracturing, drill-bit selection, wellbore stability, fault reactivation, and reservoir compaction (**Gutierrex and Lewis, 1998; Pattillo et al., 1998; Bruno, 2001; Barkved et al., 2003; Zhang, 2011; Wang et al., 2016**). During long-term production, sandstone reservoirs may experience compaction and sand production, causing reductions in permeability, reservoir pressure, and output. Therefore, knowing geomechanical properties is crucial for optimizing hydrocarbon recovery (**Settari and Walters, 2001; Zhou et al., 2016; Najibi et al., 2017; Radwan and Sen, 2021**). Geomechanical issues can arise during exploration, evaluation, development, production, and secondary recovery stages (**Zoback 2007; Liu et al., 2017**). In petroleum rock mechanics, attention is mainly focused on rocks with significant porosity and permeability. In such porous systems, pore pressure is a key factor in mechanical behaviour (**Gutierrex and Lewis, 1998; Fjaer et al., 2008**). Geomechanics controls rock deformation, which in turn influences porosity and permeability (**Gutierrex and Lewis, 1998**). Carbonate pore types form through depositional processes, diagenesis, and fracturing, and their distribution does not always match depositional facies (**Ahr, 2008; Tavakoli et al., 2018; Moeini et al., 2023; Davoodi et al., 2024; Ghorbani et al., 2025; Asadolahi Shad et al., 2026**). Due to diverse fabrics and diagenetic overprints, carbonate pore systems can be highly complex (**Tonietto et al., 2014; Hosseinzadeh and Tavakoli, 2025**). Understanding carbonate porosity requires identifying pore characteristics and linking genetic pore types to petrophysical behaviour, as well as evaluating how pore-forming processes modify rock properties (**Ahr, 2008; Sharifi-Yazdi et al., 2019; Soleimani and Tavakoli, 2023; Karimkhani and Tavakoli, 2025**). In carbonate rocks, initial porosity

* Corresponding author: Vahid Tavakoli
e-mail address: vtavakoli@ut.ac.ir
Received: 12 December 2025. Accepted: 02 May 2026.
Available online: 26 October 2026

Table 1: Summary of prior research and the unique contributions of this article

Authors	Study area	Key approaches	The key result for this paper from the previous studies
(Tavakoli et al., 2011)	South Pars gas field	wireline logs, core, thin sections, scanning electron microscopy (SEM)	Pore spaces are classified into three groups: including depositional, fabric-selective, and non-fabric-selective.
(Nazemi et al., 2018)	South Pars gas field	58 core plug samples for FRF tests, a total of 1300 porosity and permeability data, 1306 thin sections, and wireline log data	6 pore facies were determined, whereas 3 of them are more abundant (pore facies4> pore facies2 > pore facies 1) in the studied units.
(Jeng et al., 2004)	northern and western Taiwan within the Western Foothill Range	A total of 13 sandstones, obtained from 8 different geological formations, the specimens were cored in the laboratory from rock blocks	grain area ratio and porosity are the two key parameters influencing UCS and R, likewise, smaller porosity and greater grain area ratio would result in greater UCS
This paper's novelties			
Study area	**Key approaches**	**Aim and novelty**	
Persian Gulf	Cores, thin sections, routine core analysis, wireline logs,	Predicting the porosity as missing data by using AI	
Persian Gulf	Cores, thin sections, routine core analysis, wireline logs, geomechanical data	Investigating the effect of pore types on geomechanical features	

strongly influences unconfined compressive strength (UCS) in cohesive media (**Baud et al., 2014; Ng and Santamarina, 2023**). General correlations also exist between porosity, UCS, and Young's modulus (**Farquhar et al., 1994; Askaripour et al., 2022**). Other geomechanical parameters – such as fracture intensity, drilling rate, and failure style – are also controlled by porosity. Dynamic elastic modulus typically decreases with higher porosity in carbonates (**Farquhar et al., 1994; Edimann et al., 1998**). Porosity is therefore a valuable geomechanical index for addressing petroleum-related rock mechanics challenges, including wellbore stability, sand-production prediction, rock-mass classification, drilling optimization, and perforation evaluation (**Farquhar et al., 1994; Akhter and Ahmed, 2025; Kibikas et al., 2025**).

Porosity is a well-known factor in geomechanical studies, but the specific types of pore structures also play a critical role. This research focuses on carbonate rocks that contain a wide variety of pore types, each influencing their physical and mechanical behaviour differently. The main goal is to systematically evaluate how these pore structures affect key geomechanical properties. By examining the relationship between pore geometry and mechanical response, the study provides insights into the stability and deformation behaviour of carbonate formations under different stress and environmental conditions. These insights are also useful in fields such as mining, tunneling, and natural hazard assessment, where the structural stability of rock masses is essential. A clearer understanding of pore-type effects supports advancements in carbonate rock mechanics and offers practical benefits across multiple industries. This knowledge is also important for enhanced oil recovery (EOR), where pore types influence reservoir performance. In CO_2 injection and carbon-storage projects, understanding how pore types relate to geomechanical properties is crucial for evaluating storage capacity and long-term formation stability. **Table 1** presents previous studies alongside the innovations and objectives of this work.

2. Geological setting and stratigraphy

The richest oil and gas reservoirs in the world are located in the Persian Gulf Basin (see **Figure 1a**) (**Abdolmaleki and Tavakoli, 2016; Naderi-Khujin et al., 2016; Jodeyri-Agaii et al., 2018; Naderi-Khujin et al., 2020; Mohsenipour et al., 2022; Shabani et al., 2022**). In 1990, the largest non-associated gas accumulation was discovered in this area (see **Figure 1a**) (**Aali and Rahmani, 2012**). In this field, most of the gas is found within the rock layers from the Permian–Triassic period (see **Figure 1b**) (**Habibnia et al., 2016; Rafiei et al., 2016**). The Faraghan (Early Permian), Dalan (Late Permian), and Kangan (Early Triassic) formations collectively form the Permian–Triassic sedimentary succession (**Nazemi et al., 2021; Hosseinzadeh and Tavakoli, 2024**). The Dalan Formation exceeds 630 meters in thickness and is categorized into three sub-members: lower, middle, and upper. The middle sub-member, known as the Nar Member, primarily consists of anhydrite. This formation is unconformably overlain by the

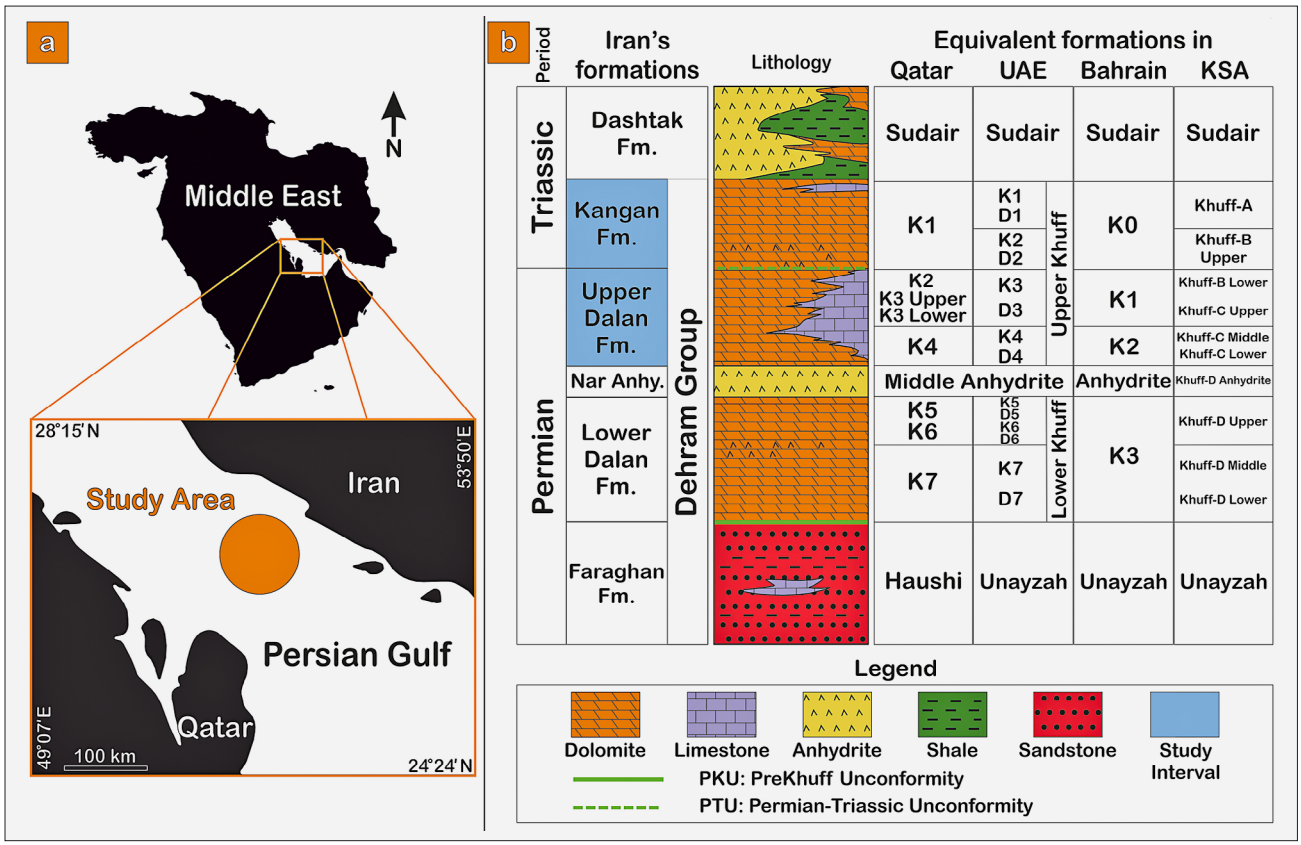


Figure 1: The study area's geographical location (a) and stratigraphy of the Dalan and Kangan formations (b), modified from **Kaveh-Ahangar et al., 2023**.

Kangan Formation (see **Figure 1b**). The Kangan Formation, with an average thickness of approximately 210 meters, comprises carbonate sediments in its lower member and shaly sediments in its upper member. These sediments were deposited unconformably on the Dalan Formation during the Early Triassic (**Haghighat et al., 2020; Rezvannia et al., 2025**). The carbonate member includes anhydritic dolomites, dolomites, limestone, and limy dolomites (see **Figure 1b**) (**Adelzadeh et al. 2014; Nikbin et al. 2021; Nafisi and Tavakoli, 2023**).

3. Materials and methods

The data used in this study include petrographical analysis from thin sections, routine core analysis, wireline logs, and geomechanical measurements, all obtained from a single well in the central Persian Gulf. The petrography data were obtained from 1577 thin sections from 403 meters of cores. Wireline log data were collected from the same interval, and geomechanical data were derived from uniaxial and triaxial tests on core samples. Geomechanical data include Young modulus (E), Poisson's ratio (ϑ), shear modulus (G), bulk modulus (K), Schmidt hammer, unconfined compressive stress (UCS), Cohesion (C), and Internal Friction Angle (Φ). Thin-section studies were conducted to identify pore types and pore facies. Porosity has been calculated by the routine core analysis tests and Boyle's law. Since porosity was not measured at some depths, the missing values were predicted using the ExtraTreesRegressor machine-learning model. Petrographic data and wireline logs were used as independent variables (X), and core porosity from routine core analysis served as the dependent variable (Y). After training and testing the model, the missing porosity values were estimated with an accuracy of 0.83. The static geomechanical moduli were then generated at the depths where petrographic data were available, allowing for comparison of the effects of pore types and diagenesis on geomechanical properties. Geomechanical dynamic moduli including E, UCS, ϑ, C, and Φ were calculated by **Equations 1 to 5**.

$$E(dynamic) = \frac{\rho_b v_s^2 \left(3v_p^2 - 4v_s^2\right)}{\left(v_p^2 - v_s^2\right)}$$

Fjaer et al., 2008 (1)

$$UCS = (7682/\Delta t)^{1.82}/145$$

Chang et al., 2006 (2)

$$\vartheta(dynamic) = \frac{(v_p^2 - 2v_s^2)}{2\left(v_p^2 - v_s^2\right)}$$

Zoback, 2007 (3)

$$\Phi = 49.03 - 1.26\,\varphi$$

Ameen et al., 2009 (4)

$$C = \frac{UCS\cos\Phi}{2(1-\sin\Phi)}$$

Radwan and Sen, 2021 (5)

Using static and dynamic data from uniaxial and triaxial test analysis on core samples, a linear regression model was developed to convert dynamic moduli to static moduli. Subsequently, the dynamic moduli, calculated by the above equations for the core samples, were converted to static moduli. The static shear modulus (G) and static bulk modulus (K) were calculated by **Equations 6** and **7**, respectively.

$$G(static) = \frac{E(static)}{2\left(1+\vartheta_{(static)}\right)}$$

Goodman, 1991 (6)

$$K(static) = \frac{E(static)}{3\left(1-2\vartheta_{(static)}\right)}$$

Archer and Rasouli, 2012 (7)

A linear regression model was developed to estimate the static internal friction angle and static cohesive strength from dynamic and static data obtained through triaxial core analyses. The model converted dynamic parameters into their static equivalents. The resulting geomechanical data were then interpolated to the depths where petrographic observations were available. A combined DataFrame was constructed, containing petrographic data, geomechanical statistics, and core-derived porosity. To remove the influence of porosity magnitude and focus solely on the effect of pore type, the dataset was partitioned based on porosity values. The goal was to ensure that samples within each group had only minor porosity differences, so that variations in geomechanical properties would primarily reflect pore type rather than porosity amount. Initially, several grouping strategies were tested. Dividing porosity into 5% intervals was too coarse, as differences in porosity still dominated the results. Using 2% intervals produced similar outcomes to the 3% grouping but caused unnecessary data scattering. Therefore, 3% intervals were selected as the optimal balance. Based on this approach, porosity was divided into consecutive 3% intervals (e.g. 0–3%, 3–6%, 6–9%, etc.). This method effectively minimized the impact of porosity magnitude and allowed clearer evaluation of pore-type effects. Since the dataset contained a wide variety of pore structures, it was necessary to classify them into meaningful categories to create pore-type facies. This grouping allowed the different pore structures to be compared consistently. We selected a classification system that organizes pore types based on pore size, connectivity, and genetic origin, factors that are particularly important when evaluating geomechanical behaviour. Since pore geometry and connectivity strongly influence mechanical strength and deformation, using a classification previously established and validated in carbonate studies was essential. Therefore, pore types were grouped into three categories: depositional pores (interparticle, fenestral, and intraparticle), fabric-selective pores (moldic and intercrystalline), and non-fabric-selective pores (fractures, stylolitic pores, intercrystalline pores, and vugs). This classification provided a reliable framework for examining how different pore structures control geomechanical properties (**Ahr, 2008; Tonietto et al., 2014; Soleimani and Tavakoli, 2023**). Intercrystalline pores were assigned to either fabric-selective or non-fabric-selective categories based on their origin and spatial distribution (**Tavakoli and Meidani, 2026**). Each row of the DataFrame represents a specific depth and includes petrographic observations, routine core analysis results, and geomechanical data (supplementary material). The constructed DataFrame contained 1,574 samples, and a bar-plot visualization was generated for each sample, which was then used in the interpretation of the results. The use of bar plots allows the data to be presented visually, which facilitates clearer interpretation and comparison of the results. Interpretation of these barplots allowed identification of the geomechanical impact of different pore types.

4. Results

4.1. Construction of pore facies

Pore facies (PF) designation is an innovative approach to classifying reservoir rocks based on the features of their pore systems. Typically, pore facies are identified by examining multiple pore types, although they can also consist of just a single pore type (**Nazemi et al., 2018; Mohsin et al., 2023**). The study of pore types and then the construction of pore facies was the first step in this research. The pore types were studied by thin-section samples. The identified pore types include interparticle, fenestral, intraparticle, moldic, intercrystalline, fracture, and vuggy. The pore facies were divided into three primary categories based on the work of Tavakoli and his colleagues (**Tavakoli et al., 2011**). The identified pore facies include depositional pores (interparticle, fenestral, intraparticle), fabric-selective pores (moldic, intercrystalline), and nonfabric-selective pores (fracture, stylolite, vuggy, intercrystalline). To predict the pore-type effects on geomechanical features, the porosity effect must be naturalized. Porosity played a key role in this study, as the DataFrame was divided based on porosity to compensate for its influence on geomechanical properties. Therefore, missing porosity values needed to be estimated. To address this, the ExtraTrees-Regressor model from the scikit-learn library was ap-

plied to predict the missing values (see **Figure 2**) (**supplementary material**). To select the most appropriate regression model, several candidate algorithms were evaluated using a k-fold cross-validation procedure. Different models, including Linear Regression, Ridge, Lasso, Random Forest, and ExtraTreesRegressor, were trained and tested through repeated data partitioning. Cross-validation was used because it provides a reliable and unbiased assessment of model performance by ensuring that all data points are used for both training and testing. Among the tested models, the ExtraTreesRegressor yielded the highest average R^2 score and showed more stable performance across the folds. Therefore, this model was selected as the optimal choice. Cross-validation is widely regarded as one of the most robust approaches for model selection, ensuring that the chosen algorithm generalizes well and avoids overfitting. Additionally, the results were validated using the GridSearchCV method. In this study, increasing the number of input data as the variable X enhanced the accuracy of the constructed model. Consequently, data obtained from thin-section analysis – including petrography, depositional environment, sedimentary facies, and diagenetic processes – as well as porosity-related log data (NPHI, DTCO, PEFZ, and RHOZ), were used as independent variables (X). Porosity was defined as the dependent variable (Y) (**supplementary material**). The test size number for this model was defined as 0.1; therefore, 10 percent of the data was used for testing the model. Since the data obtained from thin-section samples differ in depth from the data obtained from logs, the log data must be interpolated to match the depth of the thin sections. For this purpose, the Radial Basis Function (RBF) method from the interpolation module of the SciPy library was applied, as it provided the best results among the tested interpolation techniques (**supplementary material**). Finally, the model's R^2 was 0.99 for training data and 0.83 for test data (see **Figure 2**) (**supplementary material**). The hyperparameters of the model were optimized using the GridSearchCV method, which yielded a

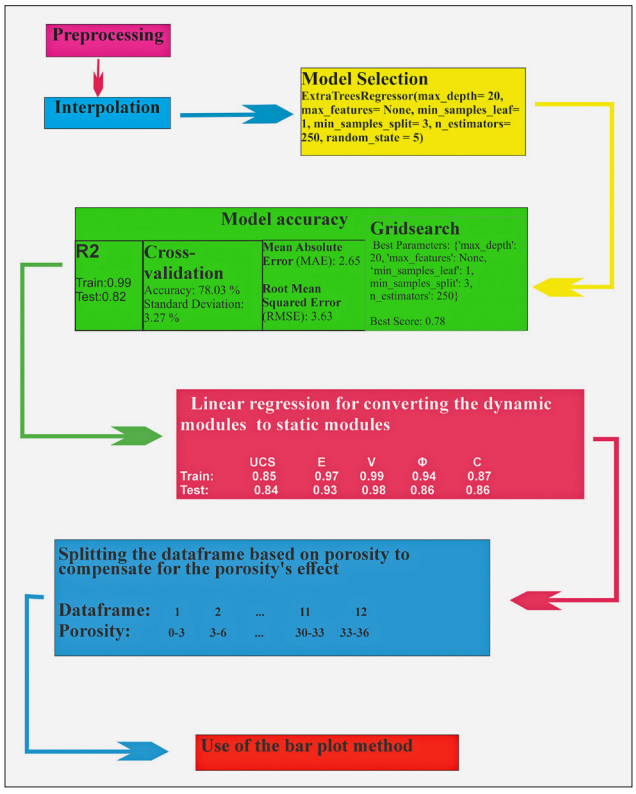


Figure 2: A flowchart illustrating the steps of using AI and its accuracy for the interpretation of the pore-type effect on geomechanical features.

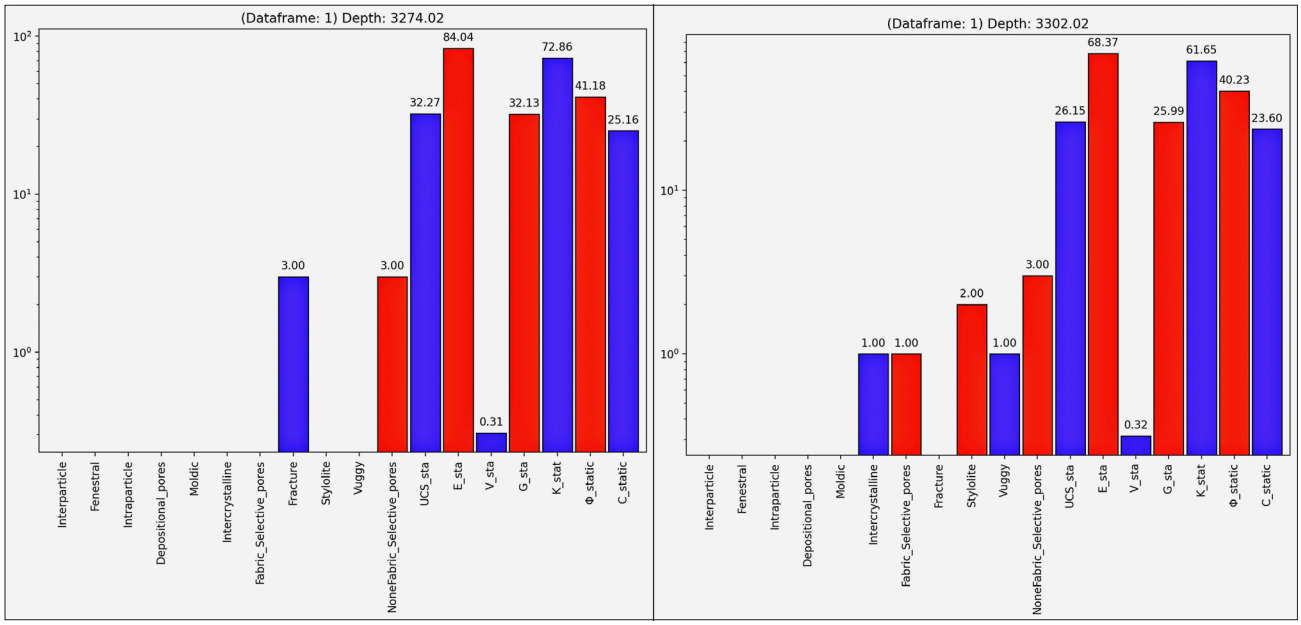


Figure 3: The effect of non-fabric selective pore type on geomechanical features. The horizontal axis in this figure represents the pore types and geomechanical moduli, while the vertical axis shows the values of these parameters.

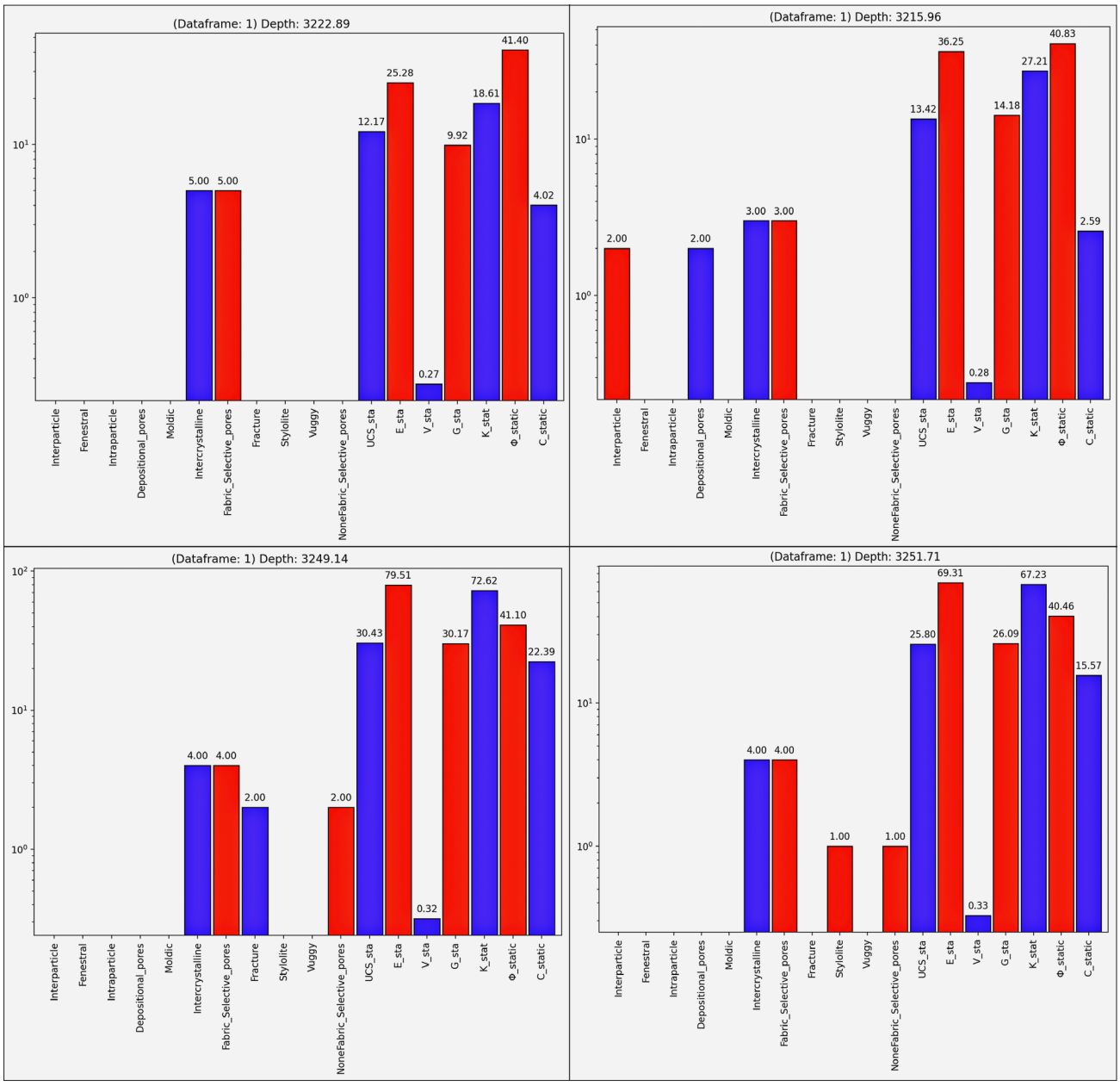


Figure 4: The effect of fabric-selective pore type on geomechanical features

best score of 0.78 (see **Figure 2**) (**supplementary material**). To further evaluate the model's accuracy, cross-validation, mean absolute error (MAE), and root mean square error (RMSE) were used (see **Figure 2**) (**supplementary material**).

4.2. Static geomechanical moduli

The geomechanical data obtained from uniaxial and triaxial tests on core samples represent static moduli. Therefore, it was necessary to calculate dynamic geomechanical moduli using sonic log data at petrographic depths. These dynamic moduli were then converted to static moduli using linear regression. The dynamic geomechanical moduli were computed using the aforementioned equations and subsequently converted to static moduli via linear regression. The R^2 for the linear regression is shown in **Figure 2**. Each module shows two R^2 which belong to the train and test data.

4.3. Geomechanical variation across pore types

The DataFrame, which had been created by petrography studies, routine core analysis results, and geomechanical data (**supplementary material**), was divided into 12 DataFrames by values of porosity. The data were grouped into separate DataFrames using porosity intervals of 3% (see **Figure 2**). To predict the effect of pore type on geomechanical characteristics, a bar plot was created for each row in the DataFrame, allowing for a comparison across different samples. To achieve this, the barplot method was applied to all samples. **Figure 3**

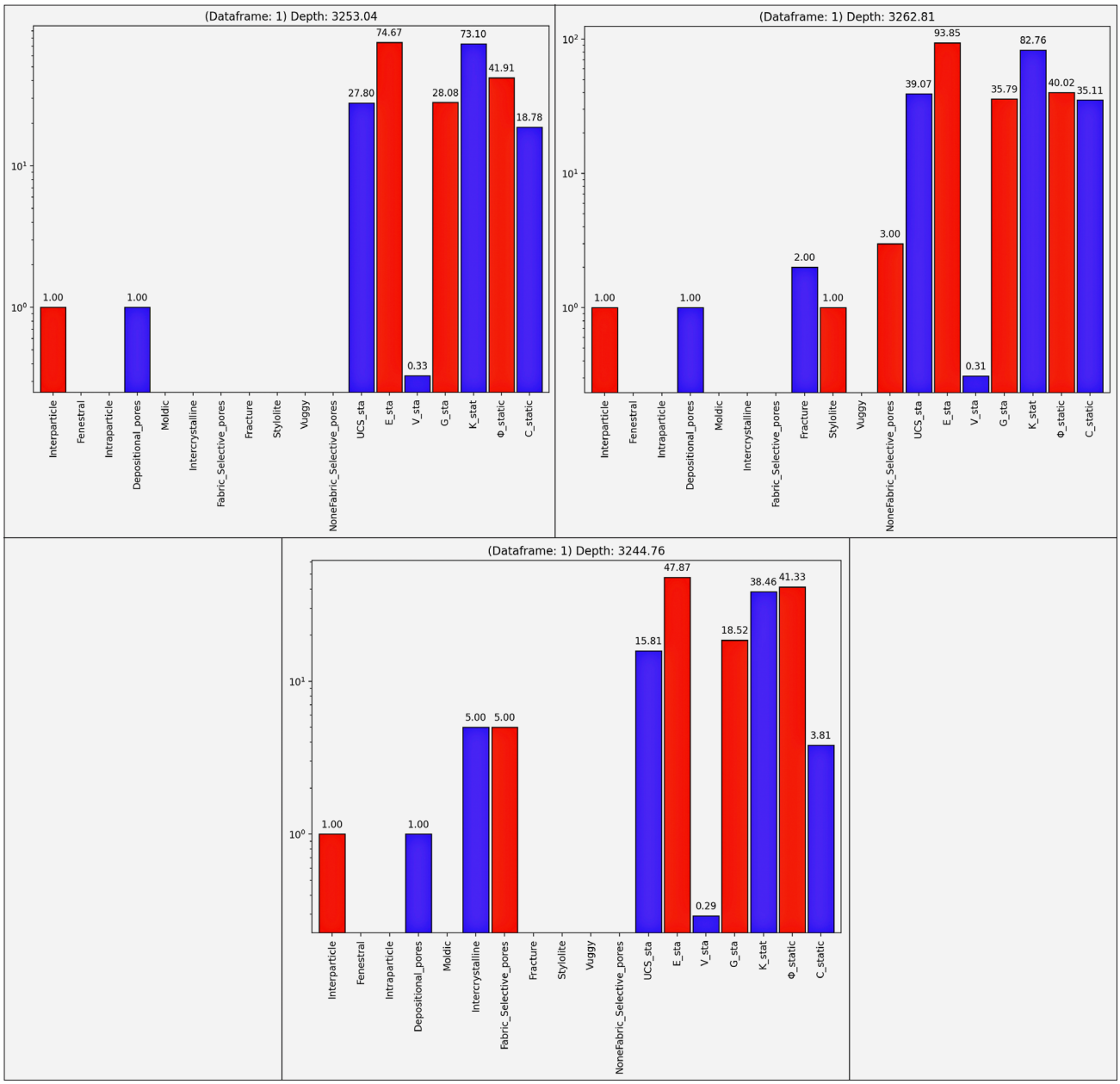


Figure 5: The effect of depositional pore type on geomechanical characteristics

shows the geomechanical moduli for the non-fabric selective pore type within the 0–3% porosity range (sample: 3274.02). In the non-fabric selective pore type, accompanied by the fabric-selective pore type, the geomechanical moduli have changed to UCS (26.15 MPa), E (68.37 GPa), ϑ (0.32%), G (25.99GPa), K (61.65 GPa), Φ (40.23 degrees), and C (23.60 MPa) (see **Figure 4,** sample: 3302.02).

The geomechanical characteristics in a sample with fabric-selective pore type are shown in **Figure 4** (sample: 3222.89). **Figure 5** (sample: 3215.96) shows the values of geomechanical moduli in a sample with fabric-selective pore type, which is accompanied by depositional pore type. By altering the value of the non-fabric selective pore type in two samples with similar fabric-selective pore type values, the geomechanical properties also changed. These shifts include UCS from 30.43 MPa to 25.80 MPa, Young's modulus (E) from 79.51 GPa to 69.31 GPa, Poisson's ratio (ϑ) from 0.32 to 0.33, shear modulus (G) from 30.17 GPa to 26.09 GPa, bulk modulus (K) from 72.62 GPa to 67.23 GPa, internal friction angle (Φ) from 41.10° to 40.46°, and cohesion (C) from 22.39 MPa to 15.57 MPa (**Figure 5**, sample depth: 3249.14) **(Figure 4,** sample: 3251.71).

The values of geomechanical features observed in a sample with depositional pore type are shown in **Figure 5** (sample: 3253.04). In one sample with a depositional pore type accompanied by a non-fabric selective pore type, and another sample with a depositional pore type accompanied by a fabric-selective pore type, the geomechanical properties differ significantly. For the first sample (see **Figure 5**, depth: 3262.81), the values are: UCS = 39.07

Table 2: The effect of non-fabric selective pores, either accompanied by fabric-selective pore type and depositional pore type, or without them, on geomechanical characteristics

Data Frame Number		2	3	4	5	6	7	8	9	10	11	12
DataFrame Porosity (%)		3-6	6-9	9-12	12-15	15-18	18-21	21-24	24-27	27-30	30-33	33-36
Geomechanical moduli value												
Without any other pores	UCS	36.34	33.82	38.19	25.84	35.62	26.46	28.12	22.48	15.75	17.73	13.94
	E	87.80	85.56	91.42	74.29	86.98	68.22	75.44	62.01	48.59	51.10	39.91
	ϑ	0.31	0.30	0.30	0.30	0.32	0.32	0.30	0.31	0.27	0.29	0.27
	G	33.40	32.83	35.06	28.58	33.05	25.89	28.97	23.70	19.10	19.88	15.72
	K	78.85	72.33	77.59	61.86	78.73	62.38	63.50	53.88	35.49	39.71	28.83
	Φ	38.05	35.33	31.08	29.45	24.59	21.90	19.24	17.42	12.34	11.53	7.84
	C	25.43	23.28	24.21	14.90	24.02	13.52	12.26	12.90	2.70	2.59	2.81
Accompanied by a Fabric-selective pore	UCS	25.02	27.29	20.31	12.13	21.75	12.32	12.42	13.01	12.28	13.05	_
	E	70.33	76.45	60.25	21.66	63.04	27.37	29.08	30.18	24.86	32.02	_
	ϑ	0.31	0.30	0.29	0.28	0.29	0.28	0.28	0.30	0.29	0.28	_
	G	26.82	29.42	23.42	8.44	24.37	10.68	11.36	11.65	9.67	12.49	_
	K	62	63.50	46.97	16.59	50.82	20.90	22.02	24.56	19.29	24.46	_
	Φ	38.02	35.03	31.88	28.08	25.97	21.88	20.79	16.67	12.69	11.25	_
	C	16.52	16.49	6.89	4.63	7.99	4.13	3.93	3.08	4.41	3.02	_
Accompanied by Depositional pore	UCS	27.24	30.64	32.10	24.13	27.87	16.68	13.35	14.37	14.01	13.79	13.43
	E	74.79	80.93	83.28	68.88	76.22	48.82	31.54	41.82	39.35	38.42	37.17
	ϑ	0.33	0.31	0.31	0.30	0.32	0.29	0.29	0.26	0.26	0.27	0.27
	G	28.11	30.96	31.90	26.57	28.84	18.90	12.25	16.57	15.56	15.11	14.64
	K	73.40	69.90	71.28	56.40	71.04	38	24.64	29.26	27.86	28.02	26.89
	Φ	39.24	36.26	33.35	28.71	26.86	22.63	19.55	16.10	13.97	8.94	6.43
	C	17.69	22.13	21.87	11.32	14.99	3.89	2.82	3.00	2.59	2.76	5.56

MPa, E = 93.85 GPa, ϑ = 0.31, G = 35.79 GPa, K = 82.76 GPa, Φ = 40.02°, and C = 35.11 MPa. In contrast, the second sample (see **Figure 5**, depth: 3244.76) shows UCS = 15.81 MPa, E = 47.87 GPa, ϑ = 0.29, G = 18.52 GPa, K = 38.46 GPa, Φ = 41.33°, and C = 3.81 MPa.

The bar plot results for DataFrame 1 are shown in the bar plot figures, while the results for DataFrames 2 to 12 are summarized in **Table 2**. This table illustrates the impact of non-fabric selective pore types, whether accompanied by depositional and fabric-selective pore types or without depositional and fabric-selective pore types, on geomechanical characteristics.

5. Discussion

5.1. Construction of porosity by AI

To predict porosity, several regression algorithms were evaluated and optimized using GridSearchCV. Among them, the ExtraTreesRegressor achieved the highest accuracy. At first, only petrographic features with high correlation to porosity were used as independent variables (X), but the model accuracy was insufficient. Incorporating all petrographic variables increased R^2 to 0.74. Adding wireline logs strongly influenced by porosity, such as NPHI, DTCO, PEFZ, and RHOZ, further improved the model accuracy to 0.82 (see **Figure 2**). This confirms that increasing the number of relevant independent variables enhances model performance. **Figure 2** summarizes the model evaluation metrics, including R^2, cross-validation, MAE, and GridSearchCV results, all indicating stable performance and reliable accuracy. This workflow is effective and can be applied to other well-logging datasets to estimate missing or costly-to-measure parameters with high precision. For converting dynamic moduli to static values, LinearRegression produced the best results among the scikit-learn linear models. In some cases, such as UCSstatic and Cstatic, polynomial features combined with linear regression provided the highest accuracy (supplementary material). The RBF interpolation method also performed best for transferring static core-derived data from wireline log depth to petrography depth, demonstrating strong effectiveness for larger datasets.

5.2. *Investigation of pore types effects on geomechanical features.*

5.2.1. Non-fabric selective pore type

A sample containing only non-fabric-selective pores showed the highest geomechanical properties (see **Figure 3**, sample 3274.02). When a non-fabric-selective pore type was accompanied by a fabric-selective pore type, the geomechanical properties decreased noticeably (see **Figure 4**, sample 3302.02). The reductions were 18% in UCS, 18% in E, 19% in G, 15% in K, 2% in Φ, and 6% in C. Overall, samples dominated by non-fabric-selective pores consistently exhibited higher geomechanical values. This is largely because fracture-related pores typically have low porosity but high permeability, which enhances mechanical strength. Accordingly, the non-fabric-selective pore facies, characterized by lower porosity compared to other facies, show higher geomechanical characteristics due to the intrinsic nature of their pore structure.

5.2.2. Fabric-selective pore type

A sample with fabric-selective pore type has the lowest geomechanical characteristics (**Figure 3,** sample: 3222.89). When a sample contains both fabric-selective and depositional pore types, the geomechanical properties increase by 10 % for UCS, 43 % for E, 42 % for G, and 46 % for K (see **Figure 3,** sample 3215.96). The geomechanical properties of a sample containing fabric-selective pores accompanied by non-fabric-selective pores are shown in **Figure 4** (**sample: 3249.14**). Similarly, in another sample with fabric-selective porosity comparable to that of sample 3249.14 but a lower non-fabric selective porosity value, the geomechanical properties are reduced (see **Figure 3,** sample 3251.71). Therefore, with decreasing the non-fabric selective pore type, the geomechanical characteristics decrease in the amount of UCS (15 %), E (7 %), G (13 %), K (7 %), Φ (1%), and C (30%). As a result, by decreasing the non-fabric selective pores, the geomechanical features are reduced. Consequently, it can be concluded that samples with fabric-selective pores – such as moldic and intercrystalline – tend to have higher porosity than other pore facies, which in turn leads to reduced geomechanical properties.

5.2.3. Depositional pore type

It can be deduced that samples containing only depositional pores exhibit higher geomechanical properties compared to those with only fabric-selective pores. Similarly, it has lower geomechanical characteristics than a sample with only non-fabric selective pores (see **Figure 4,** sample 3253.04). A sample containing both depositional and non-fabric selective pores exhibits the geomechanical characteristics presented in **Figure 4** (sample: 3262.81). Therefore, the geomechanical characteristics in a sample that has depositional pore type accompanied by non-fabric selective pore type increase in the amount of UCS (40%), E (25%), G (27%), K (13%), and C (86 %). When depositional and fabric-selective pore types coexist in a sample, the geomechanical properties decrease compared to samples containing only depositional pores. Specifically, the reductions are as follows: UCS (43%), E (35%), ϑ (12%), G (34%), K (47%), and C (79%) (see **Figure 4,** sample: 3244.76). Therefore, samples with depositional pores generally have porosity values between those of fabric-selective and non-fabric-selective pore types. Consequently, their geomechanical properties are higher than those of the former but lower than those of the latter.

As porosity increases from 1 to 12 in the DataFrames, geomechanical features decrease (see **Table 1**). This trend holds true across all DataFrames. Therefore, the consistent results across all DataFrames indicate that the effect of porosity has been effectively compensated.

5.3. *Comparison with previous studies*

Carbonates are strongly heterogeneous from various aspects (**Omrani and Tavakoli, 2024; Saadat et al., 2024; Akbarzadeh et al., 2025; Hezarkhani and Tavakoli, 2025; Shahkaram et al., 2025**). Therefore, recent advances in reservoir geomechanics have increasingly emphasized the integration of machine learning techniques with conventional petrophysical and geophysical datasets to improve the prediction and characterization of subsurface mechanical properties. For example, **Lee et al. (2025)** demonstrated that deep learning architectures, such as bidirectional long short-term memory networks, can successfully capture nonlinear relationships between well logs and geomechanical parameters, leading to accurate predictions of elastic properties such as Young's modulus, shear modulus, and bulk modulus. Similarly, **Yalamanchi et al. (2025)** highlighted the effectiveness of ensemble machine learning models in predicting pore pressure with very high accuracy, emphasizing the importance of selecting key input variables from petrophysical logs. More advanced workflows have also integrated seismic attributes with machine learning algorithms to model spatial variations in pore pressure and associated geomechanical properties in heterogeneous reservoirs (**Ehsan et al., 2025**). In addition, the application of interpretable machine learning techniques has been shown to improve the understanding of the controlling parameters on wellbore stability and effective stress behaviour, particularly when combined with poroelastic frameworks such as Biot's theory (**Fahool et al., 2023**). Despite these significant developments, most previous studies have primarily focused on predicting geomechanical parameters from log-derived or seismic data, with limited attention to the fundamental geological controls governing these properties. In particular, the role of pore type and its relationship with depositional facies and diagenetic processes has not

been sufficiently incorporated into geomechanical analyses. In this context, the present study introduces an integrated workflow that explicitly links pore types, identified through petrographic analysis, with geomechanical properties derived from core measurements and well logs. Unlike previous approaches that primarily rely on predictive modelling, this study combines machine learning techniques with geological interpretation to evaluate the impact of pore system variability on rock mechanical behaviour. The use of data-driven methods, including interpolation techniques and ensemble-based regression models, allows for the harmonization of datasets with different sampling scales and enhances the robustness of the analysis.

6. Conclusions

To account for the effect of pore type on geomechanical characteristics, the DataFrame was normalized by dividing each value by the porosity. The optimum number for dividing the porosity in this study was defined as 3. In some samples, the porosity had not been recorded. To address this issue, porosity was accurately predicted using the ExtraTreesRegressor model. Among all regression methods tested from the scikit-learn library, ExtraTreesRegressor delivered the best results in this study. As the number of independent data (X) inputs into the model increased, the R^2 value also improved, reaching 0.82. To convert dynamic moduli into static moduli, the LinearRegression model – sometimes combined with polynomial features – yielded the best results among all models tested from the scikit-learn library. In a sample with only non-fabric selective pore facies, the geomechanical features were at the highest amount. In a sample with non-fabric selective pore facies accompanied by fabric selective pore facies, the geomechanical properties were at the lowest amount. Likewise, in a sample with a non-fabric selective pore facies accompanied by a depositional pore facies, the geomechanical features were lower than in a sample with only a non-fabric selective pore facies. On the other hand, it was higher than a sample with non-fabric selective pore facies, accompanied by fabric-selective pore facies. Therefore, it was shown that the non-fabric selective pore facies have the highest geomechanical characteristics. The fabric-selective pore facies have the lowest geomechanical features, and the geomechanical characteristics in the depositional pore facies are higher than the fabric-selective pore facies and lower than the non-fabric-selective pore facies. With an increase in the porosity in the DataFrame from 1 to 12, the geomechanical characteristics were reduced, due to the increase in porosity.

7. References

Aali, J. & Rahmani, O. (2012). H2S – origin in South Pars gas field from Persian Gulf, Iran. *Journal of Petroleum Science and Engineering*, 86–87, 217–224. https://doi.org/10.1016/j.petrol.2012.03.009

Abdolmaleki, J., & Tavakoli, V. (2016). Anachronistic facies in the Early Triassic successions of the Persian Gulf and its palaeoenvironmental reconstruction. *Palaeogeography, Palaeoclimatology, Palaeoecology*, 446, 213–224. https://doi.org/10.1016/j.palaeo.2016.01.031

Adelzadeh, M. R. Hatampour, A. & Ghiasi-Freez, J. (2014). Hydrocarbon potential of Kangan and Dalan formations using organic geochemistry, mineralogy, and petrography. *Petroleum Science and Technology*, 32(18), 2159–2167. https://doi.org/10.1080/10916466.2012.755193

Ahr, W. M. (2008). A new genetic classification of carbonate porosity and its application to reservoir characterization. In AAPG Annual Convention, San Antonio, Texas, April 20–23.

Akbarzadeh, S., Davoodi, S., & Tavakoli, V. (2026). The role of facies–diagenesis interactions in shaping geomechanical heterogeneity and mechanical stratigraphy of carbonate reservoirs: Sarvak Formation, southern Iran. *Journal of African Earth Sciences*, 235, Article 105968. https://doi.org/10.1016/j.jafrearsci.2025.105968

Akbarzadeh, S., Davoodi, S., Hosseinzadeh, S., & Tavakoli, V. (2025). Integrated sedimentological and petrophysical analyses for improved reservoir characterization in the sequence stratigraphy framework: Fahliyan Formation, southwest Iran. *Journal of African Earth Sciences*, 229, Article 105699. https://doi.org/10.1016/j.jafrearsci.2025.105699

Akhter, N., & Ahmed, N. (2025). Karst collapse mechanism in the Margala Hill Limestone, Pakistan: Insights from petrography, geochemistry, isotopes, and rock mechanics. *Carbonates and Evaporites*, 40(4), Article 149. https://doi.org/10.1007/s13146-025-01186-x

Ameen, M. S. Smart, B. G. D. Somerville, J. Mc. Hamilton, S. A. & Naji, N. A. (2009). Predicting rock mechanical properties of carbonates from wireline logs (a case study: Arab-D reservoir, Ghawar field, Saudi Arabia). *Marine and Petroleum Geology*, 26(4), 430–444. https://doi.org/10.1016/j.marpetgeo.2009.01.017

Archer, S. & Rasouli, V. (2012). A log based analysis to estimate mechanical properties and in-situ stresses in a shale gas well in North Perth Basin. *WIT Transactions on Engineering Sciences*, 81, 163–174. https://doi.org/10.2495/PMR120151

Asadolahi Shad, S., Davoodi, S., & Tavakoli, V. (2026). Impact of paleotopography on carbonate reservoir heterogeneity in the Kangan Formation: A comparative research in the central and western Persian Gulf using the Winland method. *Journal of African Earth Sciences*, 235, Article 105977. https://doi.org/10.1016/j.jafrearsci.2025.105977

Askaripour, M. Saeidi, A. Mercier-Langevin, P. & Rouleau, A. (2022). A review of relationship between texture characteristics and mechanical properties of rock. *Geotechnics*, 2(1), 262–296. https://doi.org/10.3390/geotechnics2010012

Barkved, Olav, Pete Heavey, Roar Kjelstadli, Tore Kleppan, and Tron Golder Kristiansen. (2003). 'Valhall Field-Still on Plateau after 20 Years of Production'. In SPE Offshore Europe Conference and Exhibition, SPE-83957. SPE.

Baud, P. Wong, T.-F. & Zhu, W. (2014). Effects of porosity and crack density on the compressive strength of rocks. *International Journal of Rock Mechanics and Mining Sciences*, 67, 202–211. https://doi.org/10.1016/j.ijrmms.2013.08.031

Bruno, M. S. (2001). Geomechanical analysis and decision analysis for mitigating compaction related casing damage. In SPE Annual Technical Conference and Exhibition, SPE-71695. SPE.

Chang, C. Zoback, M. D. & Khaksar, A. (2006). Empirical relations between rock strength and physical properties in sedimentary rocks. *Journal of Petroleum Science and Engineering*, 51(3–4), 223–237. https://doi.org/10.1016/j.petrol.2006.01.003

Davoodi, S., Asadolahi Shad, S., & Tavakoli, V. (2024). A fresh look at the Lucia classification using mud- and grain-dominated reservoirs of the Persian Gulf. *Geoenergy Science and Engineering*, 232, Article 212437. https://doi.org/10.1016/j.geoen.2023.212437

Edimann, K. Somerville, J. M. Smart, B. G. D. Hamilton, S. A. & Crawford, B. R. (1998). Predicting rock mechanical properties from wireline porosities. In SPE / ISRM Rock Mechanics in Petroleum Engineering, SPE-47344. SPE.

Ehsan, M. Manzoor, U. Chen, R. Hussain, M. Abdelrahman, K. Radwan, A.E. Ullah, J. Iftikhar, M.K. & Arshad, F. (2025). Pore pressure prediction based on conventional well logs and seismic data using an advanced machine learning approach. *Journal of Rock Mechanics and Geotechnical Engineering*, 17(5), 2727–2740. https://doi.org/10.1016/j.jrmge.2024.09.049

Fahool, F. Shirinabadi, R. & Moarefvand, P. (2023). A case study for evaluating effective geomechanical parameters and the influence of the Biot coefficient on the stability of a wellbore wall in the Asmari Formation using machine learning. *Trends in Sciences*, 20(12), 7036. https://doi.org/10.48048/tis.2023.7036

Farquhar, R. A. Somerville, J. M. & Smart, B. G. D. (1994). Porosity as a geomechanical indicator: an application of core and log data and rock mechanics. In SPE Europec Featured at EAGE Conference and Exhibition, SPE-28853. SPE.

Fjaer, E. Holt, R. M., Horsrud, P. & Raaen, A. M. (2008). Petroleum related rock mechanics. Elsevier.

Goodman, R. E. 1991. *Introduction to Rock Mechanics*. John Wiley & Sons.

Ghorbani, B., Tavakoli, V., Rahimpour-Bonab, H., & Vahidimotlagh, N. (2025). Oil–oil and oil–source correlations in the Abadan Plain, SW Iran: Updated insights into Middle Jurassic–Lower Cretaceous petroleum systems through biomarker analysis and chemometrics. *Journal of African Earth Sciences*, 223, Article 105525. https://doi.org/10.1016/j.jafrearsci.2024.105525

Gutierrex, M. & Lewis, R. W. (1998). The role of geomechanics in reservoir simulation. In SPE/ISRM Rock Mechanics in Petroleum Engineering, SPE-47392-MS. SPE. https://doi.org/10.2118/47392-MS

Habibnia, B. Hosseini, E., Miri, R. Neshat, J. & Amiri-Bakhtiar, H. (2016). Study of Dashtak and Kangan formations boundary using geological and well log data in South Pars and Kish gas fields located in the Persian Gulf. In 3rd International Conference on Research in Science and Technology, Berlin, Germany, 1–13.

Haghighat, N., Hashemi, H., Tavakoli, V., & Nestell, G. P. (2020). Permian–Triassic extinction pattern revealed by foraminifers and geochemical records in the central Persian Gulf, southern Iran. *Palaeogeography, Palaeoclimatology, Palaeoecology*, 543, Article 109588. https://doi.org/10.1016/j.palaeo.2020.109588

Hamid, O. Omair, A. & Guizada, P. (2017). Reservoir geomechanics in carbonates. In SPE Middle East Oil and Gas Show and Conference, D041S046R003. SPE. https://doi.org/10.2118/183704-MS

Hezarkhani, Y., & Tavakoli, V. (2025). Heterogeneity dynamics: Influencing rock type responses to overburden pressure, Permian–Triassic of the Persian Gulf. *Petroleum Science and Technology*, 43(21), 2982–3001. https://doi.org/10.1080/10916466.2024.2410372

Hosseinzadeh, M., & Tavakoli, V. (2024). Analyzing the impact of geological features on reservoir heterogeneity using heterogeneity logs: A case study of Permian reservoirs in the Persian Gulf. *Geoenergy Science and Engineering*, 237, Article 212810. https://doi.org/10.1016/j.geoen.2024.212810

Hosseinzadeh, M., & Tavakoli, V. (2025). Introducing an innovative method for assessing reservoir heterogeneity using Zenga index in the Permian Basin of the central Persian Gulf. SPE Journal, 30(5), 2587–2602. https://doi.org/10.2118/225454-PA

Jeng, F.-S. Weng, M.-C. Lin, M. L. & Huang, T. H. (2004). Influence of petrographic parameters on geotechnical properties of Tertiary sandstones from Taiwan. *Engineering Geology*, 73(1–2), 71–91. https://doi.org/10.1016/j.enggeo.2003.12.001

Jodeyri-Agaii, R., Rahimpour-Bonab, H., Tavakoli, V., Kadkhodaie-Ilkhchi, R., & Yousefpour, M.-R. (2018). Integrated approach for zonation of a mid-Cenomanian carbonate reservoir in a sequence stratigraphic framework. *Geologica Acta*, 16(3), 321–337. https://doi.org/10.1344/GeologicaActa2018.16.3.5

Karimkhani, S. Tavakoli, V. Cheshomi, A. & Rahimpour-Bonab, H. (2025). Constructing a geomechanical conceptual model for Permian–Triassic reservoirs of the Persian Gulf. *Bulletin of Engineering Geology and the Environment*, 84(3), Article 140. https://doi.org/10.1007/s10064-025-04166-6

Kaveh-Ahangar, S., Nozaem, R., & Tavakoli, V. (2023). The effects of planar structures on reservoir quality of the Triassic Kangan Formation in the central Persian Gulf: An integrated approach. *Journal of African Earth Sciences*, 197, Article 104764. https://doi.org/10.1016/j.jafrearsci.2022.104764

Kibikas, W. Wilson, J. Broome, S. & Downs, C. (2025). Geomechanical characterization of Rock Valley carbonates. *Acta Geotechnica*, 20(12), 6679–6697. https://doi.org/10.1007/s11440-025-02786-6

Lee, J. Chen, Y. Dommisse, R. Saad, O.M. Huang, G.-C.D. & Savvaidis, A. (2025). Enhanced prediction of S-wave ve-

locity and geomechanical properties using depth-ordered recurrent neural networks: A case study in West Texas. *Geophysics*, 90(5), B301–B321. https://doi.org/10.1190/GEO2024-0030.1

Liu, J. Ding, W. Yang, H. Wang, R. Yin, S. Li, A. & Fu, F. (2017). 3D geomechanical modeling and numerical simulation of in-situ stress fields in shale reservoirs: A case study of the Lower Cambrian Niutitang Formation in the Cen'gong Block, South China. *Tectonophysics*, 712–713, 663–683. https://doi.org/10.1016/j.tecto.2017.06.030

Moeini, M., Rahimpour-Bonab, H., & Tavakoli, V. (2023). Evidence for isolated platform development in the Cenomanian on the passive margin of Neotethys, southwest Iran. *Minerals*, 13(6), Article 757. https://doi.org/10.3390/min13060757

Mohsenipour, A. Zahmatkesh, I. & Soleimani, B. (2022). Fractures analysis using core data and image logs: A case study in the Dalan–Kangan reservoir of South Pars Gas Field, Iran. *Iranian Journal of Science and Technology*, Transactions A: Science, 46(3), 819–828. https://doi.org/10.1007/s40995-022-01288-4

Mohsin, M., Tavakoli, V., & Jamalian, A. (2023). The effects of heterogeneity on pressure-derived porosity changes in carbonate reservoirs: Mishrif Formation in southeastern Iraq. *Petroleum Science and Technology*, 41(8), 898–915. https://doi.org/10.1080/10916466.2022.2070210

Naderi-Khujin, M., Seyrafian, A., Vaziri-Moghaddam, H., & Tavakoli, V. (2016). Characterization of the Late Aptian top-Dariyan disconformity surface offshore SW Iran: A multi-proxy approach. *Journal of Petroleum Geology*, 39(3), 269–286. https://doi.org/10.1111/jpg.12646

Naderi-Khujin, M., Tavakoli, V., Seyrafian, A., & Vaziri-Moghaddam, H. (2020). How a mud-dominated ramp changed to a carbonate–clastic oil reservoir: Sea-level fluctuations in the Cretaceous of the central Persian Gulf. *Marine and Petroleum Geology*, 116, Article 104301. https://doi.org/10.1016/j.marpetgeo.2020.104301

Nafisi, F. & Tavakoli, V. (2023). The role of textural parameters of industrial core CT scan images in detecting the petrophysical characteristics of carbonate reservoirs, Permian Dalan Formation, the central Persian Gulf. *Geoenergy Science and Engineering*, 230, Article 212277. https://doi.org/10.1016/j.geoen.2023.212277

Najibi, A. R. Ghafoori, M. Lashkaripour, G. R. & Asef, M. R. (2017). Reservoir geomechanical modeling: In-situ stress, pore pressure, and mud design. *Journal of Petroleum Science and Engineering*, 151, 31–39. https://doi.org/10.1016/j.petrol.2017.01.045

Nazemi, M. Tavakoli, V. Rahimpour-Bonab, H. Hosseini, M. & Sharifi-Yazdi, M. (2018). The effect of carbonate reservoir heterogeneity on Archie's exponents (a and m), an example from Kangan and Dalan gas formations in the central Persian Gulf. *Journal of Natural Gas Science and Engineering*, 59, 297–308. https://doi.org/10.1016/j.jngse.2018.09.007

Nazemi, M., Tavakoli, V., Rahimpour-Bonab, H., & Sharifi-Yazdi, M. (2021). Integrating petrophysical attributes with saturation data in a geological framework, Permian–Triassic reservoirs of the central Persian Gulf. *Journal of African Earth Sciences*, 179, Article 104203. https://doi.org/10.1016/j.jafrearsci.2021.104203

Ng, K. & Santamarina, J. C. (2023). Mechanical and hydraulic properties of carbonate rock: The critical role of porosity. *Journal of Rock Mechanics and Geotechnical Engineering*, 15(4), 814–825. https://doi.org/10.1016/j.jrmge.2022.07.017

Nikbin, M. Khanehbad, M. Moussavi-Harami, R. Mahboubi, A. Khoddami, M. & Ghofrani, E. (2021). Porosity system analysis and its relation to the permeability of the reservoir zones in the Upper Dalan Member and Kangan Formation: A case study, one of the gas fields in the Zagros Coastal Fars, SW Iran. *Journal of Petroleum Science and Engineering*, 196, 107835. https://doi.org/10.1016/j.petrol.2020.107835

Omrani, S., & Tavakoli, V. (2024). Influences of geological and petrophysical attributes on electrical resistivity–based reserve evaluation: Enhancing carbonate reservoir classification, Permian–Triassic reservoirs of southern Iran. *SPE Journal*, 29(10), 5352–5371. https://doi.org/10.2118/223075-PA

Pattillo, P. D. Kristiansen, T. G. Sund, G. V. & Kjelstadli, R. M. (1998). Reservoir compaction and seafloor subsidence at Valhall. In SPE/ISRM Rock Mechanics in Petroleum Engineering (Eurock '98), Trondheim, Norway, SPE-47274. SPE. https://doi.org/10.2118/47274-MS

Radwan, A. E. A. & Sen, S. (2021). Stress path analysis for characterization of in situ stress state and effect of reservoir depletion on present-day stress magnitudes: Reservoir geomechanical modeling in the Gulf of Suez rift basin, Egypt. *Natural Resources Research*, 30(1), 463–478. https://doi.org/10.1007/s11053-020-09731-2

Rafiei, M., Rahimpour-Bonab, H., Tavakoli, V., & Khorasani, E. (2016). Quantifying sedimentary and diagenetic controls on fracturing: An application in rock engineering systems. *Journal of Geophysics and Engineering*, 13(6), 928–939. https://doi.org/10.1088/1742-2132/13/6/928

Rezvannia, F. Mosaddegh, H. Biranvand, B. Nestell, G. P. & Tavakoli, V. (2025). Late Permian–Early Triassic transition in the carbonate–evaporite strata of the eastern part of the Qatar–Fars Arch, Persian Gulf basin. *Marine and Petroleum Geology*, 181, Article 107524. https://doi.org/10.1016/j.marpetgeo.2025.107524

Saadat, K., Rahimpour-Bonab, H., Tavakoli, V., & Gholinezhad, J. (2024). Experimental investigation and prediction of saturation exponent in carbonate rocks: The significance of rock–fluid properties. *Journal of Petroleum Exploration and Production Technology*, 14, 149–163. https://doi.org/10.1007/s13202-023-01714-2

Settari, A. & Walters, D. A. (2001). Advances in coupled geomechanical and reservoir modeling with applications to reservoir compaction. *SPE Journal*, 6(3), 334–342. https://doi.org/10.2118/74142-PA

Settari, A., and Sen, V. (2008). Geomechanics in Integrated Reservoir Modeling. Paper presented at the Offshore Technology Conference, Houston, Texas, USA, May 2008. doi: https://doi.org/10.4043/19530-MS

Shabani, F., Amini, A., Tavakoli, V., Honarmand, J., & Gong, C. (2022). 3D forward stratigraphic modeling of the Albian succession in a part of the northeastern margin of the Arabian Plate and its implications for exploration of subtle traps. *Marine and Petroleum Geology*, 145, Article 105880. https://doi.org/10.1016/j.marpetgeo.2022.105880

Shahkaram, M., Aleali, M., Tavakoli, V., & Maleki, Z. (2025). Comparative analysis of Permian–Triassic sequences in the eastern Persian Gulf: Insights into their paleoenvironments and diagenetic history. *Iranian Journal of Earth Sciences*, 17(3), Article 172520. https://doi.org/10.57647/j.ijes.2025.16786

Sharifi-Yazdi, M., Rahimpour-Bonab, H., Tavakoli, V., Nazemi, M., & Kamali, M. R. (2019). Linking diagenetic history to depositional attributes in a high-frequency sequence stratigraphic framework: A case from Upper Jurassic Arab Formation in the central Persian Gulf. *Journal of African Earth Sciences*, 153, 91–110. https://doi.org/10.1016/j.jafrearsci.2019.02.006

Soleimani, A. & Tavakoli, V. (2023). The application of equivalent pore aspect ratio (EPAR) in detecting the pore types and determining rock types, Kangan and Dalan formations, Persian Gulf. *Journal of Petroleum Geomechanics*, 6(4), 16–24. https://doi.org/10.22107/JPG.2023.404591.1199

Tavakoli, V. (2016). Ocean chemistry revealed by mineralogical and geochemical evidence at the Permian–Triassic mass extinction, offshore the Persian Gulf, Iran. *Acta Geologica Sinica* (English Edition), 90(5), 1852–1864. https://doi.org/10.1111/1755-6724.12821

Tavakoli, V. Rahimpour-Bonab, H. & Esrafili-Dizaji, B. (2011). Diagenetic controlled reservoir quality of South Pars gas field, an integrated approach. *Comptes Rendus Geoscience*, 343(1), 55–71. https://doi.org/10.1016/j.crte.2010.10.004

Tavakoli, V., & Meidani, B. (2026). Why conventional velocity rules break down: Geological and petrophysical controls on sonic response in Permian–Triassic carbonate reservoirs, southern Iran. *Journal of African Earth Sciences*, 237, Article 106033. https://doi.org/10.1016/j.jafrearsci.2026.106033

Tavakoli, V., Naderi-Khujin, M., & Seyedmehdi, Z. (2018). The end-Permian regression in the western Tethys: Sedimentological and geochemical evidence from offshore the Persian Gulf, Iran. *Geo-Marine Letters*, 38(2), 179–192. https://doi.org/10.1007/s00367-017-0520-8

Tonietto, S. N. Smoot, M. Z. & Pope, M. (2014). PS pore type characterization and classification in carbonate reservoirs. *Search and Discovery Article* #41432, American Association of Petroleum Geologists.

Wang, Z. Gao, D. & Liu, J. (2016). Multi-objective sidetracking horizontal well trajectory optimization in cluster wells based on DS algorithm. *Journal of Petroleum Science and Engineering*, 147, 771–778. https://doi.org/10.1016/j.petrol.2016.09.046

Yalamanchi, P. Datta Gupta, S. & Upadhyay, R. (2025). Evaluating the effectiveness of ensemble machine learning approaches for pore pressure prediction using petrophysical log data in carbonate reservoir. *Acta Geophysica*, 73(3), 2591–2619. https://doi.org/10.1007/s11600-025-01530-8

Zhang, J. (2011). Pore pressure prediction from well logs: Methods, modifications, and new approaches. *Earth-Science Reviews*, 108(1–2), 50–63. https://doi.org/10.1016/j.earscirev.2011.06.001

Zhou, D. Zheng, P. He, P. & Peng, J. (2016). Hydraulic fracture propagation direction during volume fracturing in unconventional reservoirs. *Journal of Petroleum Science and Engineering*, 141, 82–89. https://doi.org/10.1016/j.petrol.2016.01.028

Zoback, M. D. (2007). Reservoir geomechanics. Cambridge University Press. https://doi.org/10.1017/CBO9780511586477

SAŽETAK

Geomehanički utjecaji tipova pora identificiranih strojnim učenjem u permsko-trijaskim ležištima perzijskoga zaljeva

Za optimizaciju stabilnosti kanala bušotina, procesa bušenja i crpljenja ugljikovodika u naftnoj industriji ključno je razumijevanje geomehaničkoga ponašanja stijena. Ovim je istraživanjem ispitano kako različite vrste pora utječu na geomehanička svojstva ležišta. U istraživanju su korišteni rezulati petrografskih analiza, karotažnih mjerenja, rutinski podatci o jezgrama i rezultati geomehaničkih mjerenja. Geomehanički podatci uključuju Youngov modul elastičnosti (E), Poissonov omjer (ϑ), modul smicanja (G), modul stišljivosti (K), vrijednosti odskoka Schmidtova čekića, jednoosnu tlačnu čvrstoću (UCS), koheziju (C) i kut unutarnjega trenja (Φ). Podatkovni skup (engl. *DataFrame*) podijeljen je na temelju poroznosti kako bi se procijenio njezin utjecaj na geomehanička svojstva. Nedostajuće vrijednosti poroznosti predviđene su pomoću modela ExtraTreesRegressor, koji je postigao R^2 od 0,82. Budući da su skupovi podataka dobiveni s različitih dubina uzorkovanja, za interpolaciju geomehaničkih svojstava dobivenih karotažnim mjerenjima na dubine jezgara korištena je metoda radijalne bazne funkcije (RBF). Zatim su primijenjeni stupčasti dijagrami temeljeni na strojnome učenju kako bi se procijenio utjecaj vrste pora na geomehanička svojstva. Rezultati pokazuju da stijene s porama čiji oblik i raspored nisu određeni početnom teksturom ili sastavom sedimentata (engl. *non-fabric-selective pores*), imaju najveću geomehaničku čvrstoću. S druge strane, jezgre s porama koje ovise o izvornome sedimentnom sastavu i strukturi stijene (engl. *fabric-selective pores*) pokazuju najslabija svojstva. Stijene s primarnom poroznošću nastalom taloženjem (engl. *depositional pore types*) nalaze se između ranije navedenih. Integracijom petrografskih i petrofizičkih podataka s tehnikama strojnoga učenja ovo istraživanje daje praktičan tijek rada za procjenu geomehaničke heterogenosti. Ovakvim pristupom omogućena je bolja karakterizacija ležišta i bolje donošenje odluka u razradi polja s karbonatnim ležištima.

Ključne riječi:
vrste pora, geomehanička svojstva, strojno učenje, ExtraTreesRegressor model

Author's contribution

Saeed Karimkhani: Conceptualization, methodology, investigation, data curation, formal analysis, visualization, writing – original draft. **Vahid Tavakoli**: Supervision, conceptualization, methodology, writing – review & editing, project administration.
All authors have read and agreed to the published version of the manuscript.